Electrochemical Model-Based State of Charge Estimation for Li-Ion Cells

Matteo Corno, Nimitt Bhatt, Sergio M. Savaresi, and Michel Verhaegen

I. Introduction

BATTERIES represent the limiting factor for several applications, with electric mobility one of the most prominent. Focusing on vehicle applications, batteries have a series of drawbacks with respect to fossil fuels: they have lower energy and power density, their life is uncertain, and their behavior changes with time. In the past few years, lithium ion batteries have risen as the preferred technology for both portable devices and vehicular applications (see [1] and [2] for a more thorough analysis of Li-ion batteries).

A considerable amount of research is being devoted to batteries: research on new chemistries and new types of batteries [3]; domain-dependent research on energy management systems (e.g., vehicle energy management systems [4]) and research on battery management systems (BMSs) [5]. New chemistries promise to deliver higher energy densities; however, with the rise of electric vehicles shorter term solutions are needed. The need for immediate solutions is pushing the research into better ways of managing the available energy at the vehicle level. Vehicle-level energy management relies on the knowledge of the state of the battery and its limits. State of charge (SoC), that is, an indication of how much energy is left in the battery, is one of the most important states. It is apparently important as an indication of the vehicle range, but it has important implications on the life-cycle of the battery. It is the BMSs task to provide this information. Sophisticated BMSs are therefore necessary to ensure performance, safety and longevity. A large number of SoC estimation approaches are available in the literature. They can be classified in model-free and model-based techniques. Model-free techniques are based on heuristics, like Coulumb counting or machine-learning techniques (neural network or Fuzzy approach) [6]. Model-based techniques are based on an application of an observer (Kalman-like or sliding mode) [7] to a dynamic model of the battery.

Several battery models exist. They are classified in white-box or electrochemical models [8], [9], gray-box or electroequivalent models [10] and black-box models [11]. Currently, the most performing BMSs adopt electroequivalent models [10], [12], [13]. These models, by neglecting the mass-transfer dynamics, are computationally efficient but not very accurate during high current events. Physically based electrochemical models are needed to provide a better monitoring [14] of the internal states of the cell and higher levels of accuracy.

Material scientists have developed electrochemical models that describe the spatially distributed behavior of the states of the cell [15], [16]. These models are often used to optimize the physical design of batteries. The applicability of white-box models to BMS remains to be fully explored [17]. The main limitation is complexity. White-box models result in complex algebraic nonlinear partial differential equations (PDE) describing the distribution of the states along the spatial dimensions [18]. Electrochemical model-based BMSs need to solve those equations in real time. To tackle this issue, researchers developed *ad hoc* model reduction techniques [19]–[24]).

In this paper, we present an efficient electrochemical model-based SoC estimation approach. The key-enabling factor is recasting the high-dimensional coupled nonlinear equations in a distributed framework. This, with only minor approximations, enables the rise of the underlying semiseparable structure (SSS). The SSS [25] in turns enables the efficient manipulation of matrices. Thus, the computations needed to run an extended Kalman filter (EKF) can be considerably sped-up.

Although not common, other electrochemical model-based SoC observers have been presented in the literature, see for example [23], [26]–[28]. Compared with other methods, the presented approach has several advantages. First, the efficiency is obtained by exploiting the structure of the equations.

Manuscript received July 29, 2013; revised January 21, 2014; accepted March 9, 2014. Date of publication April 11, 2014; date of current version December 15, 2014. Manuscript received in final form March 27, 2014. Recommended by Associate Editor S. Varigonda.

M. Corno and S. M. Savaresi are with the Dipartimento di Elettronica, Informazione e Bioingegneria, Politecnico di Milano, Milan 20133, Italy (e-mail: corno@elet.polimi.it; savaresi@elet.polimi.it).

N. Bhatt and M. Verhaegen are with the Delft Center for Systems and Control, Delft University of Technology, Delft 2628 CN, The Netherlands (e-mail: nimitt28@gmail.com; m.verhaegen@tudelft.nl).

Color versions of one or more of the figures in this paper are available online.

TABLE I

GOVERNING EQUATIONS OF LI-ION CELL MODEL

Conservation Equations			Boundary Conditions	
Species				
Solid Phase	$\frac{\partial c_s}{\partial t} = \frac{D_s}{r^2}\overrightarrow{\nabla}_r\left(r^2\overrightarrow{\nabla}_r c_s\right)$	(1)	$\overrightarrow{\nabla}_r c_s\Big\|_{r=0} = 0; \quad D_s\overrightarrow{\nabla}_r c_s\Big\|_{r=R_s} = \frac{-j^{Li}}{a_s F}$	(2)
Electrolyte Phase	$\frac{\partial \epsilon_e c_e}{\partial t} = \overrightarrow{\nabla}_x\left(D_e^{eff}\overrightarrow{\nabla}_x c_e\right) + \frac{1-t_+^0}{F}j^{Li}$	(3)	$\overrightarrow{\nabla}_x c_e\Big\|_{x=0} = \overrightarrow{\nabla}_x c_e\Big\|_{x=L} = 0$	(4)
Charge				
Solid Phase	$i_s(x) = -\sigma^{eff}\overrightarrow{\nabla}_x\phi_s$	(5)	$-\sigma_-^{eff}\overrightarrow{\nabla}_x\phi_s\Big\|_{x=0} = \sigma_+^{eff}\overrightarrow{\nabla}_x\phi_s\Big\|_{x=L} = \frac{I}{A}$	(6)
			$\overrightarrow{\nabla}_x\phi_s\Big\|_{x=\delta_-} = \overrightarrow{\nabla}_x\phi_s\Big\|_{x=\delta_-+\delta_{sep}} = 0$	(7)
Electrolyte Phase	$i_e(x) = -\kappa^{eff}\overrightarrow{\nabla}_x\phi_e - \kappa_D^{eff}\overrightarrow{\nabla}_x\ln c_e$	(8)	$\overrightarrow{\nabla}_x\phi_e\Big\|_{x=0} = \overrightarrow{\nabla}_x\phi_e\Big\|_{x=L} = 0$	(9)

The basic idea of the method is thus generic. Second, compared with the two-particle models [22], a finer granularity and therefore a higher accuracy at high current can be achieved. Third, no state transformation is needed and thus variables maintain their physical meaning, making the tuning of the algorithm easier (see [21]). On the other hand, this paper shares a common drawback with other electrochemical model-based approaches. It requires the value of several physical parameters.

This paper is structured as following: in Section II the basic equations governing Li-ion cells are recalled and spatially discretized. In Section III, the derivation of an efficient control-oriented model is presented and the SSS structure revealed; in Section IV, the SoC observer is detailed discussing the observability of the system. In Section V, the method is tested, validated, and compared with another method. This paper is finally concluded in Section VI.

II. LITHIUM ION CELL MODELING

A typical Li-ion battery cell has four main components (Fig. 1): the porous negative and positive electrodes (where the active material is), the separator and the electrolyte. During discharge, Li diffuses to the surface of the active material particles and there it undergoes the electron-generating reaction. The Li^+ moves through the electrolyte to the positive electrode, where it is reabsorbed in the active material of the positive electrode. The concentration of Li and how fast it can diffuse and be absorbed determines the dynamics of the cell. In this section, the basic equations describing these phenomena will be recalled. The model follows the derivation presented in [18] and [29]. A 6 Ah Li-ion cell designed and built for the DOE FreedomCAR program is taken as a reference cell. This choice is supported by the extensive analysis carried out on this cell in [16], [18], [30], [31], and references cited within. In the following, the cell is modeled at room temperature as previously done in [30].

A. Fundamental Equations

The model consists of several PDEs where t represents the time, x the spatial coordinate along the x-direction, and r the spatial coordinate along the radius of the active material sphere. $c_e(t,x)$ represents the Li^+ concentration in the electrolyte, $c_s(t,r,x)$ the concentration of Li in the solid phase; $\phi_s(x,t)$ and $\phi_e(x,t)$ are, respectively, the potential

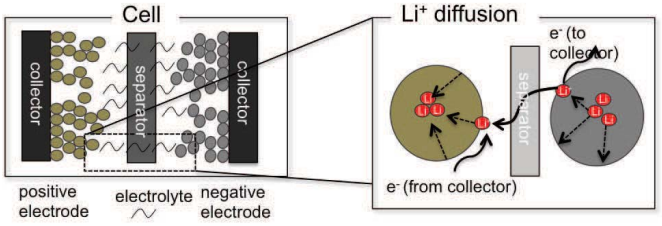

Fig. 1. Internal structure and operation of a Li-ion cell and graphical representation of the Li^+ diffusion dynamics.

in the solid and electrolyte phases. The PDEs are described in Table I. In the equations, D_s is the solid-phase diffusion coefficient; F is the Faraday's constant; a_s is the specific interfacial area of an electrode; D_e^{eff} is the effective diffusion coefficient; t_+^0 is the transference number of Li^+ with respect to the velocity of solvent which is assumed to be constant; σ^{eff} is the effective conductivity and κ^{eff} the effective ionic conductivity, while κ_D^{eff} is the effective diffusion conductivity.[1] A is the electrode plate area; $\delta_{-,\text{sep},+}$ are the thickness of the negative and positive electrodes and separator. The external current I enters or leaves the cell at the terminals. At each spherical particle interface, the current gets diverged owing to the reaction taking place between the electrode and the electrolyte. The magnitude of the current is related to the volumetric rate of electrochemical reaction taking place at the solid or electrolyte interface (j^{Li}) as

$$\overrightarrow{\nabla}_x i_s(x) = -j^{\text{Li}}; \quad \overrightarrow{\nabla}_x i_e(x) = j^{\text{Li}}. \tag{10}$$

The PDEs are coupled by the Butler-Volmer kinetics equation describing the reaction current at the solid or electrolyte interface

$$j^{\text{Li}}(x) = a_s j_0\left[\exp\left(\frac{\alpha_a F}{RT}\eta\right) - \exp\left(-\frac{\alpha_c F}{RT}\eta\right)\right] \tag{11}$$

where α_a and α_c are the anodic and cathodic transfer coefficients of electrode reaction, R is the universal gas constant, T is the absolute temperature in Kelvin, k is the kinetic rate constant, and j_0 is the exchange current density. The overpotential η is

$$\eta = \phi_s - \phi_e - U(c_{s,e}). \tag{12}$$

[1]For notational simplicity, all the model coefficients are considered to be constant in the solid phase, separator, and electrolyte phase. Note that the method is applicable also in case of spatial dependency of the parameters.

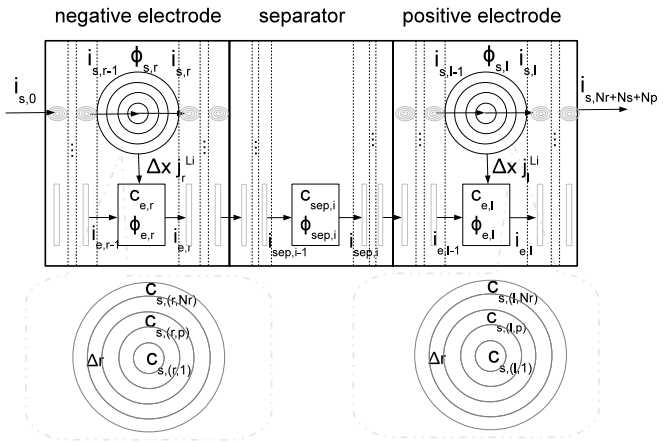

Fig. 2. Discretization of Li-ion cell along x and r dimensions.

The equilibrium (open circuit) voltage $U(c_{s,e})$ is evaluated as a nonlinear empirical function of the surface stoichiometry [18]. Further, there is no divergence of current within the separator ($x \in [\delta_-,\ \delta_- + \delta_{\text{sep}}]$.) and the entire terminal current flows through the separator in the form of Li^+

$$\overrightarrow{\nabla}_x i_e(x) = 0 \tag{13}$$

$$-\kappa^{\text{eff}} \overrightarrow{\nabla}_x \phi_e - \ \kappa_D^{\text{eff}} \overrightarrow{\nabla}_x \ln c_e \ = \frac{I}{A}. \tag{14}$$

Finally the cell potential is

$$V = \ \phi_s(x = L) - \phi_s(x = 0) - \frac{R_f}{A} I \tag{15}$$

where R_f is the film resistance on the electrodes surface.

B. Discretization

To integrate the above set of equations a spatial discretization is proposed herein. The cell is discretized as shown in Fig. 2. The model input is considered as the dis/charge current I.

A finite difference method is used to discretize the PDEs. Other methods have been presented (see [32]) to solve specific PDEs systems, the finite difference method has been chosen for its simplicity. In Fig. 2, the positive and negative electrodes are assumed to be formed of a series of spherical active material particles, each occupying one slice of the discretization along x with step Δx. Each spherical active material particle is further discretized along the radial dimension r with step Δr. N_r, N_n, N_s, and N_p are, respectively, the number of finite elements in which the sphere, the negative electrode, the separator, and the positive electrode are discretized. Each discretized region has a lumped electrolyte phase Li^+ concentration c_e and electrolyte phase potential ϕ_e (named c_{sep} and ϕ_{sep} in the separator). Each sphere has a lumped solid-phase potential ϕ_s, whereas the solid-phase Li concentration is distributed along r. The volumetric rate of electrochemical reaction, j^{Li}, is lumped in a discretized region. The currents, i_s and i_e, are also distributed along x. Dynamic equations arise from the mass balances. By discretizing (1) one obtains

$$\dot{c}_{s,(k,p)} = \frac{D_s}{(p\Delta r)^2}\left[2p\Delta r\left(\frac{c_{s,(k,p+1)} - c_{s,(k,p)}}{\Delta r}\right) + (p\Delta r)^2\left(\frac{c_{s,(k,p-1)} - 2c_{s,(k,p)} + c_{s,(k,p+1)}}{\Delta r^2}\right)\right] \tag{16}$$

with discretized boundary conditions (2)

$$c_{s,(k,1)} - c_{s,(k,0)} = 0 \tag{17}$$

$$D_s\left(\frac{c_{s,(k,N_r+1)} - c_{s,(k,N_r)}}{\Delta r}\right) = \frac{-j_k^{\text{Li}}}{a_s F}. \tag{18}$$

In the previous equation p represents the r-discretization index and k the x-discretization index. The second set of dynamic equations is obtained by discretizing the electrolyte phase mass balance

$$\dot{c}_{e,k} = \frac{D_e^{\text{eff}}}{\epsilon_e}\left(\frac{c_{e,k-1} - 2c_{e,k} + c_{e,k+1}}{\Delta x^2}\right) + \frac{1 - t_+^0}{F} j_k^{\text{Li}} \tag{19}$$

with boundary conditions

$$c_{e,1} - c_{e,0} = 0, \quad c_{e,N_s+N_n+N_p} - c_{e,N_s+N_n+N_p+1} = 0. \tag{20}$$

The Butler-Volmer kinetics provides an expression for j_k^{Li}. Equation (11) can be written for each discretized slice at the positive and negative electrode (recall that $j_k^{\text{Li}} = 0$ in the separator)

$$j_k^{\text{Li}} = \ a_s j_0\left[\exp\left(\frac{\alpha_a F}{RT}\eta_k\right) \ - \exp\left(-\frac{\alpha_c F}{RT}\eta_k\right)\right] \tag{21}$$

where $\eta_k = \phi_{s,k} - \phi_{e,k} - U\left(c_{s,(k,N_r)}\right)$.

Equation (5) is discretized as

$$-\sigma_{\pm}^{\text{eff}}\left(\frac{\phi_{s,k+1} - \phi_{s,k}}{\Delta x}\right) = i_{s,k} \tag{22}$$

with boundary conditions (6) and (7) translated in

$$i_{s,0} = \frac{I}{A}, \quad i_{s,N_n+N_s+N_p} = \frac{I}{A}$$
$$i_{s,N_n} = 0, \quad i_{s,N_n+N_s} = 0.$$

The above equations connect the solid-phase potential with the solid-phase current. The relation between the current in the solid phase and the reaction current is given by the discretization of (10)

$$i_{s,k+1} - i_{s,k} = -\Delta x j_k^{\text{Li}}. \tag{23}$$

A similar approach can be followed for the electrolyte phase potentials and currents, applying Kirchhoff's current law and using boundary conditions (9)

$$i_{e,k+1} - i_{e,k} = \Delta x_k j_k^{\text{Li}}. \tag{24}$$

Discretizing (8)

$$-\kappa_-^{\text{eff}}\left(\frac{\phi_{e,k+1} - \phi_{e,k}}{\Delta x}\right) - \kappa_{D-}^{\text{eff}}\left(\frac{\ln c_{e,k+1} - \ln c_{e,k}}{\Delta x}\right) = i_{e,k} \tag{25}$$

with boundary conditions

$$\phi_{e,1} - \phi_{e,0} = 0, \quad \phi_{e,N_n+N_p+N_s} - \phi_{e,N_n+N_p+N_s+1} = 0.$$

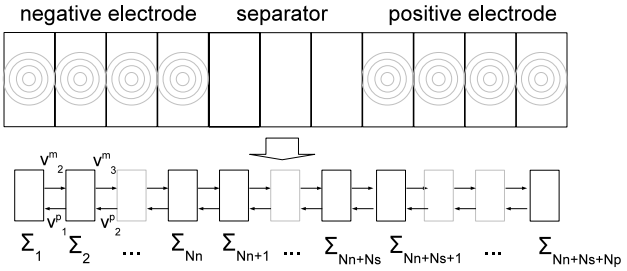

Fig. 3. Li-ion cell as spatially distributed string interconnected system.

Finally, the terminal voltage is given by the discretized version of (15)

$$V = \phi_{s,1} - \phi_{s,N_n+N_p+N_s} - \frac{R_f}{A} I. \tag{26}$$

The model has $(N_r + 1)N_p + (N_r + 1)N_n + N_s$ dynamic equations that can be solved using numerical integration; however, at each integration step, the terms j_k^{Li} need to be evaluated by solving the whole set of nonlinear algebraic system. The large dimensionality and the implicit relations make the system in this form difficult to use in practice.

Having defined the current generating reactions, the SoC can be defined as

$$\mathrm{SoC}(t) = \frac{c_{s,\mathrm{avg}}^{-}(t) - c_{s,0\%}^{-}}{c_{s,100\%}^{-} - c_{s,0\%}^{-}} \tag{27}$$

where $c_{s,\mathrm{avg}}^{-}(t)$ is the average Li concentration in the negative electrode solid phase; $c_{s,0\%}^{-}$ and $c_{s,100\%}^{-}$ are, respectively, the averaged concentration corresponding to the discharged and charged cell.

III. Computational Efficient Model

In this section, we will show how, by modeling the cell as a spatially distributed system, it is possible to efficiently simulate the system and obtain an explicit state-space model. The idea is that of dividing the cell model into subsystems that communicate through interface variables, see Fig. 3.

A. Spatially Interconnected Systems

A system that can be written as a string interconnection of N_{tot} subsystems (see Fig. 3) of the form

$$\begin{aligned} \dot{x}_k &= f_k\big(x_k, v_k^p, v_k^m, u_k\big) \\ v_{k-1}^p &= g_k^p\big(x_k, u_k, v_k^p, v_k^m\big) \\ v_{k+1}^m &= g_k^m\big(x_k, u_k, v_k^p, v_k^m\big) \\ y_k &= h_k\big(x_k, v_k^p, v_k^m, u_k\big) \end{aligned} \tag{28}$$

is said to be a spatially distributed string interconnected system (see [25] for a complete description of the properties of such systems). Let us start considering a strictly spatially proper system, that is, a system where g_k^p and g_k^m are not dependent on v_k^m and v_k^p, respectively. In this case, an explicit description of the system can be written by eliminating the interconnecting variables (also known as lifting the system), thus obtaining a $N_{\mathrm{tot}}N_{\mathrm{sub}}$ order system (N_{sub} being the order of the subsystem assumed constant for ease of exposition). The computational complexity of integrating such systems with standard ordinary differential equation (ODE) solvers grows as $O((N_{\mathrm{tot}}N_{\mathrm{sub}})^3)$. The time required to simulate the system grows quickly and the ability to use the lifted system for real-time applications may be lost. If the system is kept distributed and each subsystem simulated independently a higher efficiency can be achieved. The decoupling can be achieved by sampling the interconnecting variables at frequency h. This makes it possible to simulate the N_{tot} subsystems independently (possibly in parallel) at a shorter integration step (h_2) and let them exchange information through the interface variables only at a lower sampling rate. This approximation reduces the computational complexity to $O(N_{\mathrm{tot}}N_{\mathrm{sub}}^3)$ or even $O(N_{\mathrm{sub}}^3)$, if a parallel architecture is available. The increased efficiency may come at the cost of accuracy; however, if the subsystems have internal stiff dynamics that are weakly coupled to the dynamics of the interconnecting variables the approximation will be negligible.

Not all systems are spatially strictly proper (in particular we will see that the system at hand is indeed not strictly proper). If g_k^p or g_k^m are dependent on v_k^m and v_k^p, it is, in general, not possible to write the subsystems in explicit form. However, in case of linear dependency an efficient method is proposed hereafter. Assume that the system can be written as

$$\begin{aligned} \dot{x}_k &= f_k\big(x_k, v_k^p, v_k^m, u_k\big) \\ v_{k-1}^p &= g_{k1}(x_k, u_k) + W_k^p v_k^p + Z_k^m v_k^m \\ v_{k+1}^m &= g_{k2}(x_k, u_k) + Z_k^p v_k^p + W_k^m v_k^m \\ y_k &= h_k\big(x_k, v_k^p, v_k^m, u_k\big) \end{aligned} \tag{29}$$

then the interconnecting equations can be arranged in a linear system of the form $Ev = b(x, u)$ where

$$v = \begin{bmatrix} v_1^p \\ v_2^m \\ v_2^p \\ \vdots \\ v_{N-1}^m \\ v_{N-1}^p \\ v_N^m \end{bmatrix} \quad b = \begin{bmatrix} g_{12}(x_1, u_1) \\ g_{21}(x_2, u_2) \\ g_{22}(x_2, u_2) \\ \vdots \\ g_{(N-1)1}\big(x_{(N-1)}, u_{(N-1)}\big) \\ g_{(N-1)2}\big(x_{(N-1)}, u_{(N-1)}\big) \\ g_{N1}(x_N, u_N) \end{bmatrix}. \tag{30}$$

Computation shows that matrix E is endowed with a very specific structure. Being a SSS matrix, it can be written as

$$E = \mathrm{SSS}(L_s, M_s, N_s, O_s, P_s, Q_s, R_s) \tag{31}$$

where

$$\begin{aligned} L_s &= \begin{bmatrix} I \\ 0 \end{bmatrix} \ \forall s \in \{2, 3, \ldots, N-1\}, \ L_N = I \\ M_s &= 0 \ \forall s \in \{2, 3, \ldots, N-1\} \\ N_1 &= I, \ N_s = [\,0 \quad I\,] \ \forall s \in \{2, 3, \ldots, N-1\} \\ O_1 &= -Z_1^p, \ O_N = -Z_N^m \\ O_s &= \begin{bmatrix} -Z_s^m & -W_s^p \\ -W_s^m & -Z_s^p \end{bmatrix} \ \forall s \in \{2, 3, \ldots, N-1\} \\ P_1 &= I, \ P_s = \begin{bmatrix} 0 \\ I \end{bmatrix} \ \forall s \in \{2, 3, \ldots, N-1\} \\ Q_s &= 0 \ \forall s \in \{2, 3, \ldots, N-1\} \\ R_s &= \begin{bmatrix} I & 0 \end{bmatrix} \ \forall s \in \{2, 3, \ldots, N-1\}, \ R_N = I. \end{aligned} \tag{32}$$

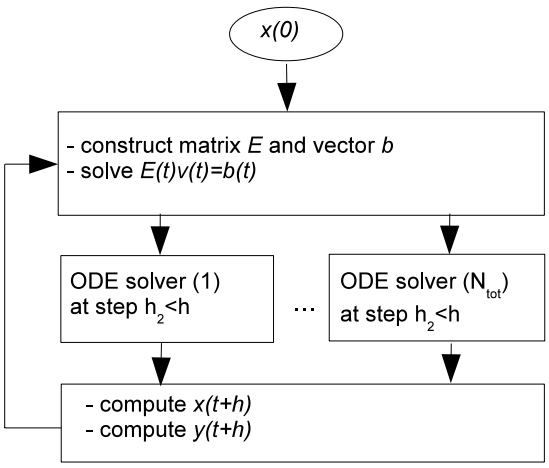

Fig. 4. Li-ion cell simulator algorithm.

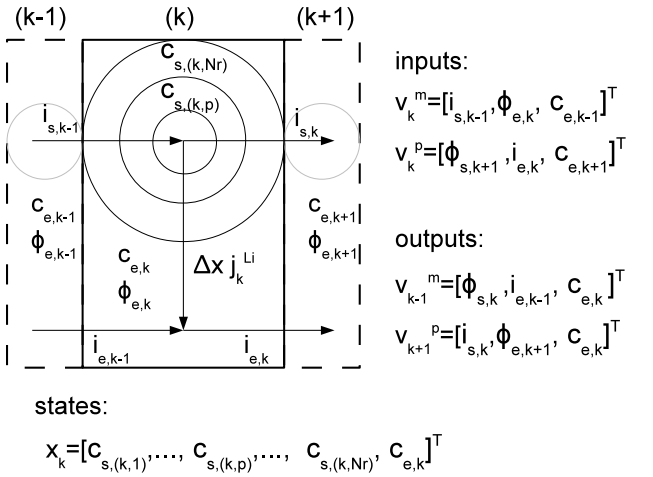

Fig. 5. Single discretized part of positive or negative electrode interconnected with neighboring blocks shown as dotted.

The SSS structure makes it possible to solve the system of equations with $O(N_{\text{tot}})$ complexity (the reader is referred to [25] for an extensive discussion of SSS matrices). If E is invertible the system is well posed [33] and the interconnecting variables can be computed in a centralized block before the integration of each subsystem.

From the above discussion, the integration routine shown in Fig. 4 is defined. At each integration step, the state-dependent parameters are updated according to the previously computed value of the states; these values are used to construct matrix E and vector b and to obtain the interconnected variables υ at a sampling step h. After that, all the subsystems can be simulated in parallel using an ODE solver of choice keeping the interconnecting variables constant.

B. Spatially Interconnected Li-Ion Cell Model

We will show how the model presented in Section II can be cast into a string interconnected system; we will focus on the details for a single central finite element of the electrodes. Fig. 5 shows the kth finite element with its input and output variables. The state equations for the subsystems are obtained from (16) and (19). There are N_r dynamic equations for the solid spherical active material particle and one equation from the electrolyte concentration. These differential equations depend on j_k^{Li} that need to be expressed as a function of states and inputs. By eliminating ϕ_{sk} from (21) using (5) and then eliminating i_{sk} using (23) an implicit function for j_k^{Li} is obtained. Linearization of (21) is used to bring the expression to an explicit form. Referring to [18] the linearized version of the Butler-Volmer kinetics is

$$j_k^{\text{Li}} = \frac{a_s}{R_{ct}}[\phi_{sk} - \phi_{ek} - U(c_{s(k,N_r)})] \tag{33}$$

where

$$R_{ct} = \frac{RT}{j_0 F(\alpha_a + \alpha_c)}.$$

Substituting this expression of j_k^{Li} in the dynamic equations, we obtain the following state equations:

$$\begin{aligned}\dot{x}_k = &\begin{bmatrix} -\alpha_1 & \alpha_1 & 0 & \dots & 0 \\ \frac{D_s}{\Delta r^2} & -\alpha_2 & \alpha_2 & \dots & 0 \\ \dots & \dots & \dots & \dots & \dots \\ 0 & \dots & \frac{D_s}{\Delta r^2} & -\frac{D_s}{\Delta r^2} & 0 \\ 0 & \dots & 0 & 0 & -\frac{2D_e^{\text{eff}}}{\epsilon_e \Delta x^2} \end{bmatrix} x_k \\ &+ \begin{bmatrix} 0 \\ 0 \\ \dots \\ -\Omega\ U\ (x_k\ (N_r)) \\ -\gamma\ \ U\ (x_k\ (N_r)) \end{bmatrix} + \begin{bmatrix} 0 & 0 & 0 \\ 0 & 0 & 0 \\ \dots & & \dots \\ \Omega & 0 & 0 \\ \gamma & 0 & \frac{D_e^{\text{eff}}}{\epsilon_e \Delta x^2} \end{bmatrix} v_k^p \\ &+ \begin{bmatrix} 0 & 0 & 0 \\ 0 & 0 & 0 \\ \dots & & \dots \\ \Omega\frac{\Delta x}{\sigma^{\text{eff}}} & -\Omega & 0 \\ \gamma\frac{\Delta x}{\sigma^{\text{eff}}} & -\gamma & \frac{D_e^{\text{eff}}}{\epsilon_e \Delta x^2} \end{bmatrix} v_k^m \end{aligned} \tag{34}$$

where

$$\Omega = -\frac{1}{\beta R_{ct}}\left(\frac{2}{N_r \Delta r F} + \frac{1}{\Delta r F}\right) \quad \gamma = \frac{a_s}{\beta R_{ct}}\left(\frac{1 - t_+^0}{F}\right)$$
$$\beta = 1 + \frac{\Delta x^2}{\sigma^{\text{eff}}}\frac{a_s}{R_{ct}} \quad \alpha_i = \left(\frac{2D_s}{i\,\Delta r} + \frac{D_s}{\Delta r^2}\right) \tag{35}$$

and, defining some constants

$$M_1 = \frac{\Delta x a_s}{\beta R_{ct}} \quad M_2 = \frac{\Delta x^2}{\sigma^{\text{eff}}}\frac{a_s}{\beta R_{ct}}$$
$$M_3 = \frac{\Delta x}{\sigma^{\text{eff}}} \quad M_4 = -\frac{\Delta x}{\kappa^{\text{eff}}} \quad K_d K = \frac{\kappa_D^{\text{eff}}}{\kappa^{\text{eff}}} \tag{36}$$

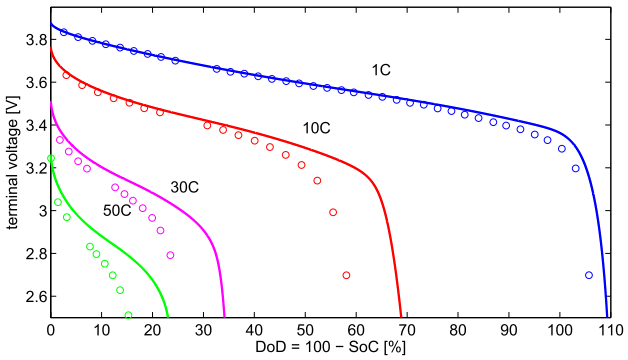

Fig. 6. Terminal voltage prediction of model at different C-rates: (-) discretized model and (o) CFD model.

the output relation equations can be derived as

$$v_{k-1}^{p} = \begin{bmatrix} M_2 U\left(x_k(N_r)\right) \\ M_1 U\left(x_k(N_r)\right) \\ x_k(N_r+1) \end{bmatrix} + \begin{bmatrix} (1-M_2) & 0 & 0 \\ -M_1 & 1 & 0 \\ 0 & 0 & 0 \end{bmatrix} v_k^p + \begin{bmatrix} M_3\,(1-M_2) & M_2 & 0 \\ -M_2 & M_1 & 0 \\ 0 & 0 & 0 \end{bmatrix} v_k^m \tag{37}$$

$$v_{k+1}^{m} = \begin{bmatrix} M_1 U\left(x_k(N_r)\right) \\ K_d K \ln\left(x_k(N_r+1)\right) \\ x_k(N_r+1) \end{bmatrix} + \begin{bmatrix} -M_1 & 0 & 0 \\ 0 & M_4 & 0 \\ 0 & 0 & 0 \end{bmatrix} v_k^p + \begin{bmatrix} -(M_2-1) & M_1 & 0 \\ 0 & 1 & 0 \\ 0 & 0 & 0 \end{bmatrix} v_k^m + \begin{bmatrix} 0 \\ -K_d K \ln\left(v_k^p(N_r)\right) \\ 0 \end{bmatrix}. \tag{38}$$

The same procedure can be applied to the separator and to the interfaces between the terminals and the electrodes and the electrodes and separator; by doing so a system in the form of (28) is obtained. From the analysis of the above system, two conclusions can be drawn. First, the interconnecting output variables are only weakly coupled to the Li diffusion in the active material; in fact only the last element $x_k(N_r)$ appears in the above equations. Second, although the subsystems are not directly in the linear in interconnecting variables form, it should be noted that the only nonlinear term depends on $v_k^p(N_r)$ which is a state of the neighboring block and is thus available for solving the system $Ev = b$. The above considerations justify the application of the method previously proposed.

The above simplifications are verified by comparing an SSS-based model ($N_r = 40$, $N_n = N_p = N_s = 3$ and $h = 0.05s$) against the 313th order CFD model also employed for validation in [18]. Three different aspects are considered.

C. Teminal Voltage Prediction

Fig. 6 shows the predicted terminal voltage at constant discharge current of 1 C, 10 C, 30 C, and 50 C from 100% initial SoC condition and the terminal voltage is plotted as a function of depth of discharge (DoD).

The model is very accurate in the entire DoD range for 1 C; for higher currents the accuracy range is reduced toward the end of discharge. The voltage-based end of discharge is predicted with at most a 12% error in SoC. This is due to the terminal voltage characteristic $U(c_{s,e})$: with high currents the solid-phase surface concentration $c_{s,e}$ is depleted to a region where $U(c_{s,e})$ is strongly nonlinear; thus small errors in $c_{s,e}$ will result into larger errors in terminal voltage.

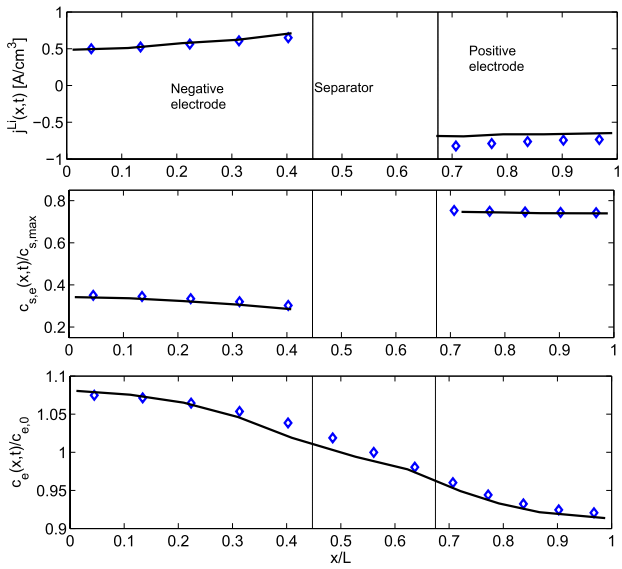

Fig. 7. Gradient of different quantities formed along the length of the cell with 5 C discharge current with 50% SoC initial condition at time = 20 s, discretized model (◇), CFD model (-).

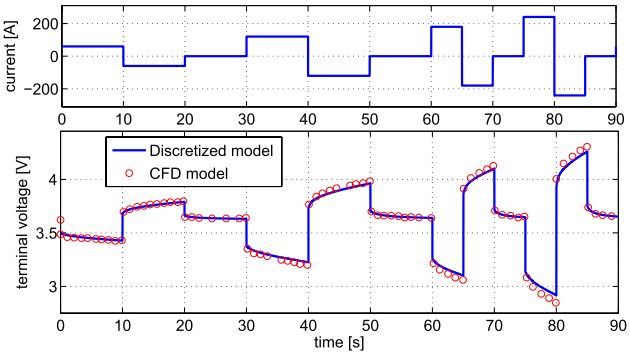

Fig. 8. Voltage response of the model with high rate charge and discharge current profile.

D. Gradients Along x

Physical-based cell models can capture the gradients of different quantities in the cell. Fig. 7 shows the validation of the proposed model in this respect.

It can be observed that the gradients are accurately captured by our model.

E. Response to Transient Current Profile

Fig. 8 validates the model for dynamically changing currents.

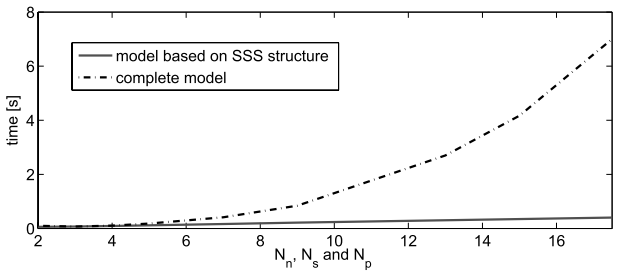

Fig. 9. Averaged simulation time to simulate 0.1 s.

From 50% initial SoC the voltage response has a maximum error of 80 mV at 40 C charge pulse and its recovers very quickly in the following rest period.

F. Complexity Analysis

The results presented refer to a rather coarse discretization; the accuracy of the model can be improved by using a finer discretization, at the expense of computational time. An analysis of simulation[2] time is presented. The integration time grows linearly with the number of finite elements along x. Fig. 9 shows the simulation time required to simulate 0.1 s of real time with different discretization levels of positive electrode, negative electrode, and separator. To avoid penalizing overhead caused by data-structure allocation, the simulation times are computed as an average of a 10 s simulation. With the proposed method, a discretization of $N_r = 40$, $N_n = 3 = N_p = N_s = 3$ requires 0.08 s to simulate 0.1 s of real time. The complete solution of the nonlinear equations presented in the section, on the other hand, requires 0.2 s to simulate 0.1 s.

In summary, the proposed modeling approach, relying only on two approximations (linearization of the Butler-Volmer kinetics and the holding of the interconnecting variables), has several advantages.

1) It provides an efficient nonlinear simulator that captures the mass diffusion dynamics of the Li-ion cell.
2) It avoids any iterative solution of nonlinear equations, thus improving efficiency and avoiding possible non convergent behavior.
3) It provides a state-space nonlinear model that can be directly employed for model-based estimation system design.
4) If linearized, the state space model assumes an SSS structure that can further exploited in the design and implementation of control systems.
5) It is amenable to parallelization, thus improving even further the computational efficiency.

IV. SoC Estimation

One of the benefits of modeling the Li-ion cell as SSS model is that the structure can be exploited to design and implement observers. It will be shown how the distributed structure can be exploited to design a SoC EKF. First, the general ideas will be present, followed by the tailoring of the approach to the SoC estimation.

[2]The simulations are performed on a 2.66 GHz Intel Core 2 Quad with 4GB memory under MATLAB.

Any EKF implementation revolves around three basic steps.

1) *Time Update:* Using the model of the system, input signal and the previously estimated value of the state, the future value of the state and output are predicted. This step consists in the integration of the modeled dynamics, as such the simulation method described in Section III is used. To improve the prediction step accuracy, the time-update is performed using a variable step integration routine.
2) *Linearization:* In this step, the model is linearized and discretized. Traditionally one would first lift the system and then perform the Jacobian computation. This implies operating on a possibly large dimension system. If the subsystems are first linearized and then lifted, the efficiency is improved (see Appendix A). At this stage, the discrete time conversion is performed obtaining matrix Φ_k that preserves the SSS structure.
3) *Correction or Measurement Update:* The most computational demanding operation in the correction or measurement update step is the computation of the Kalman gain. At each time instant k, the gain L_k is computed as

$$\Sigma^-_{\tilde{x},k} = \hat{\Phi}_k \Sigma^+_{\tilde{x},k-1} \hat{\Phi}^T_k + \Sigma_w \tag{39}$$

$$L_k = \Sigma^-_{\tilde{x},k} \hat{C}^T_k \left[\hat{C}_k \Sigma^-_{\tilde{x},k} \hat{C}^T_k + \Sigma_v\right]^{-1} \tag{40}$$

$$\Sigma^+_{\tilde{x},k} = \left(I - L_k \hat{C}_k\right) \Sigma^-_{\tilde{x},k}. \tag{41}$$

If matrix $\Sigma^+_{\tilde{x},0}$ is initialized in the SSS form as well as matrices Σ_w and Σ_v, all the steps of measurement update can be performed using the SSS arithmetic having $O(N)$ computational complexity. At the last step, the state error covariance matrix $\Sigma^+_{\tilde{x},k}$ obtained will be in the SSS form which is then used in the next iteration and thus the SSS structure is preserved through all iterations.

To apply the above method, the observability properties of the SoC dynamics need to be studied.

Linearization of the model previously described reveals that the system is not locally fully observable. In particular, three eigenvalues are not observable. The loss of observability is better understood by referring to a simplified models. The lumped model is composed of three charge tanks: the negative and positive electrodes and the electrolyte. Each of the element contains Li (ions) concentration indicated by $c_{s,\text{avg}-}$, $c_{s,\text{avg}+}$, and $c_{e,\text{avg}}$. In this simplified model, the output voltage mainly depends on the difference between $c_{s,\text{avg}-}$ and $c_{s,\text{avg}+}$. Therefore, being I and V the only available measurements, the three internal states are not independently observable. There is a infinite number of $c_{s,\text{avg}-}$ and $c_{s,\text{avg}+}$ that yields the same V.

However, the study of the complete system dynamics reveals some properties that can be exploited to improve observability. In particular, the concentration of Li-ions in the electrolyte does not vary considerably under nominal usage conditions.

Fig. 10 shows a high current rate charge/discharge test; the average concentration in the electrolyte is subject to only minimal variations when compared to the fluctuations in the negative and positive electrodes. As a consequence of the small variations of Li-ions in the electrolyte, it is also observed that

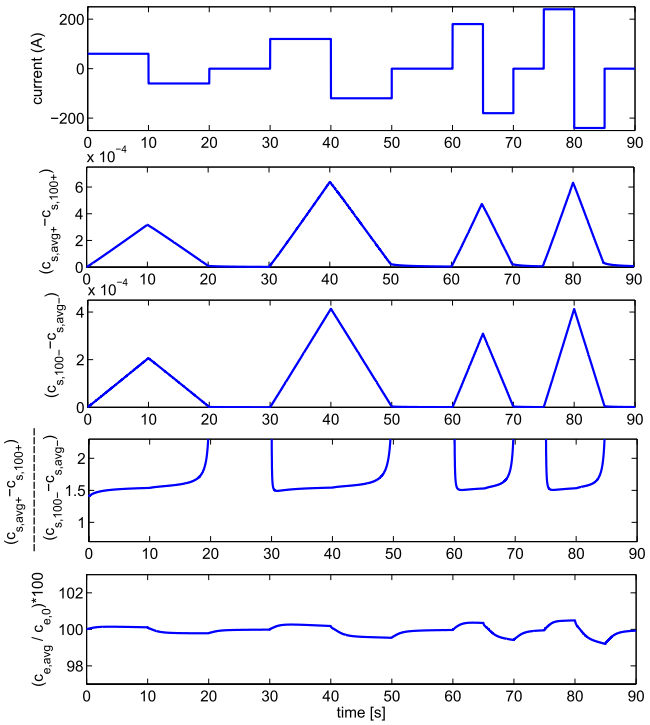

Fig. 10. Co-relation between the solid-phase average Li-ion concentration of positive and negative electrodes and percentage variance of electrolyte phase average Li^+ ion concentration about its nominal value for high rate dis/charge current profile.

the addition/removal of Li ion to the positive electrode will be similar to the removal/addition of Li-ions from the negative electrode.

If taken as algebraic constraints, the above observations lead to the so-called single particle model [28] in which the electrolyte states are dropped. This approach reduces the order of the model and simultaneously improves the observability. In the following, a different approach in undertaken; the rationale is not to use these observations as hard (algebraic) constraints, but rather to incorporate them in the Kalman filter. This improves the observability without limiting the model degrees of freedom and this potentially yields more accuracy. In particular, two virtual measurements are added.

1) The observation that $c_{e,\text{avg}}$ is roughly constant is incorporated by virtually measuring $c_{e,\text{avg}}$ and assigning it its constant nominal value identified in simulation. Note that $c_{e,\text{avg}}$ is a linear combination of the internal states of the system.
2) The consideration that the mass variation of Li in the positive and negative electrodes are similar is incorporated by adding a virtual measurement of $c_{s,\text{avg}+}(k)$ that is derived from the *a priori* prediction $c_{s,\text{avg}-}(k)$ according to

$$c_{s,\text{avg}+} = \frac{\delta_- \epsilon_{s-}}{\delta_+ \epsilon_{s+}}(c_{s,100\%-} - c_{s,\text{avg}-}) + c_{s,100+}$$

that implements the Li balance as concentrations. Also, in this case, the virtual measurement can be written as linear combination of the system states.

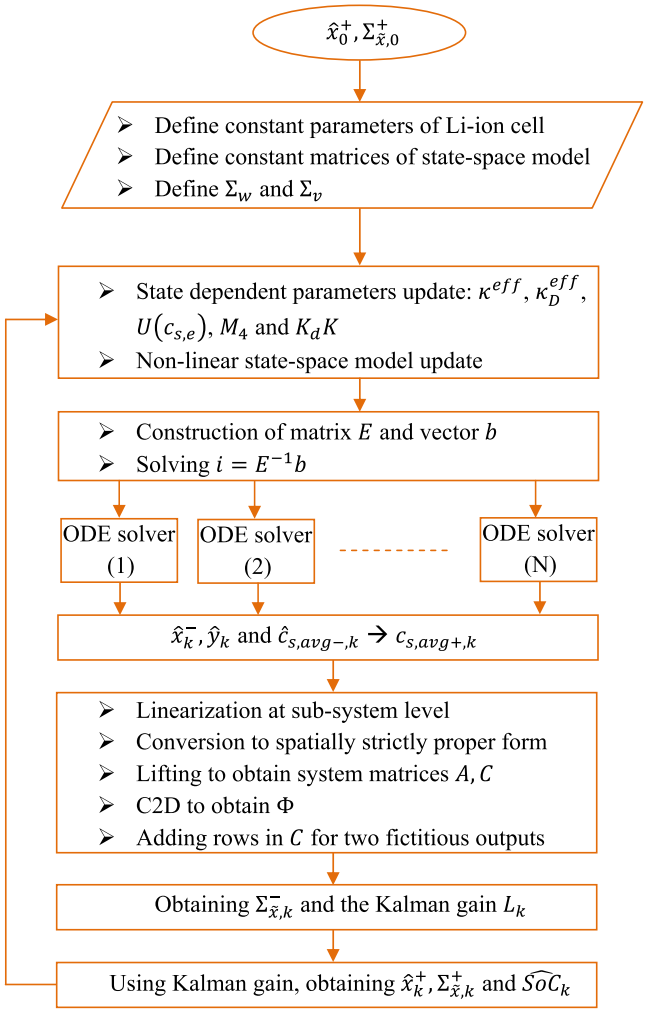

Fig. 11. SoC estimation algorithm.

Using these two virtual outputs, the system is fully locally observable. This approach is implemented as shown in Fig. 11.

The algorithm starts with an initial estimate of the state and error covariance $(\hat{x}_0^+, \Sigma_{\tilde{x},0}^+)$. Following that, the model is simulated to generate the *a priori* estimate of the state and outputs (real and virtual) $(\hat{x}_k^-, \hat{y}_k)$. After this, linearization is performed at the subsystem level, the matrices are transformed to convert the linearized interconnected system as spatially strictly proper and then using these transformed matrices as generators, the SSS form of lifted matrices A and C are obtained. Because the A matrix is obtained from linearization of continuous time state equations, it needs to be converted to the discrete time matrix Φ using the SSS-structure preserving Tustin conversion technique. Also additional rows are added to matrix C corresponding to the fictitious sensors: solid-phase average Li ion concentration in the positive electrode and electrolyte phase average Li^+ ion concentration. This step causes a loss of structure for the C which can be recuperated as shown in [25]. The EKF matrix computation steps are executed, first to obtain the Kalman gain L_k and then the corrected state estimate $\hat{x}_k^+$ along with its error covariance matrix $\Sigma_{\tilde{x},k}^+$. Finally, an estimate of the state of charge $\widehat{\text{SoC}}_k$ is derived from the corrected states. Here the SoC is derived

using (27) using the positive electrode as a reference since the equilibrium potential of positive electrode has a greater contribution in the measured output, that is, terminal voltage.

V. Simulation Results

In this section, the proposed SoC estimator is tested and compared with another model-based approach. The 6 Ah reference cell simulator demonstrated in Section III without any simplification is used as a true system. The simulation model is different from the model employed in the observer under several aspects.

1) The two-step simulation scheme is not employed, rather a variable step integration routine is used.
2) The order of the simulator is chosen higher than that of the model used in the estimator. For the simulator the following discretization is used: $N_r = 50$, $N_n = 15$, $N_p = 15$, and $N_s = 15$. The estimator, on the other hand uses the discretization analyzed in Section III, that is, $N_r = 40$, $N_n = 3$, $N_p = 3$, and $N_s = 3$.
3) An additive white Gaussian noise with a signal to noise ratio of 50 dB is added to the measurement.

Heuristics lead the tuning of EKF. Simulations show that $c_{e,\text{avg}}$ remains very close to $c_{e,0}$, with a maximum error of $\pm 3\%$ while the ratio of $(c_{s,\text{avg}+} - c_{s,100+})$ to $(c_{s,100-} - c_{s,\text{avg}-})$ is subject to wider variations, as high as $\pm 10\%$. The real measurement, terminal voltage is noisy but should be given more weight since it is the only real measurement from the system. These considerations lead to $\Sigma_v = \text{diag}([1, 1\times10^{-3}, 1\times10^{2}])$ where $y_k = [V_k, c_{e,\text{avg},k}, c_{s,\text{avg}+,k}]^T$. The process noise is modeled by $\Sigma_w = 1 \times 10^{-3} I$ while the initial state error covariance matrix is chosen I.

Two tests have been performed.

1) A discharge test estimation applying a 10 s, 10 C pulse discharge current profile starting from 100% SoC. This test is identical to the one performed in [30].
2) A more challenging charge/discharge test reaching up to 50 C.

The results of the first test are shown in Fig. 12. The following conclusions can be drawn.

1) It can be observed that in the entire range, the SoC is estimated accurately. The RMS error in the entire range is only 1.7%.
2) The approach is robust to initial condition error. A 5% initial error is reabsorbed in approximately 100 s. The convergence time increases with higher initial error.
3) The plots compare the proposed algorithm with another electrochemical SoC estimator available in literature. The reference estimator, presented in [30] and [34], is designed on the same 6 Ah reference cell and uses an *ad hoc* model reduction technique. The proposed algorithm can better estimate the SoC at low and high values.
4) The estimation algorithm is running with $h = 0.05$ s; lower sampling rates have also been tested finding that for sampling rates up to $h = 0.1$ s the estimation converges to the actual value with slightly longer settling times without the need of retuning. The use of lower sampling rates causes bigger estimation errors during fast transient that offset the advantages of using an electrochemical-based model.

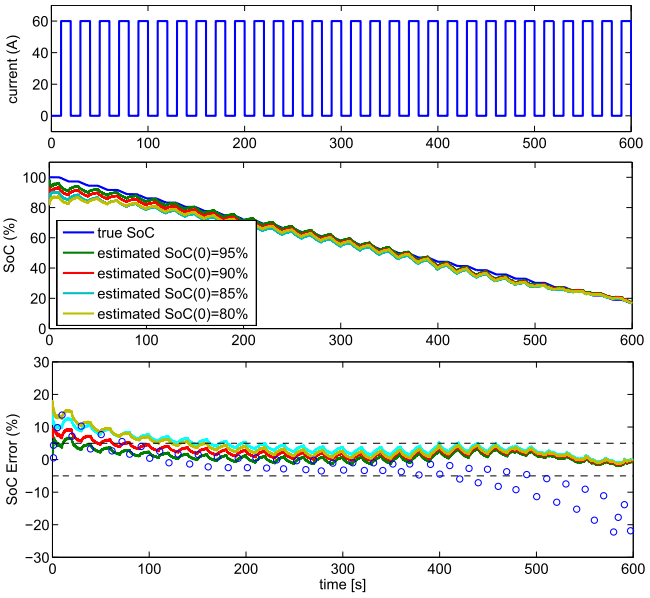

Fig. 12. SoC estimation results with a 10 s, 10 C pulse discharge current profile. Subplot (c) compares the SoC estimation error by this approach (-) against SoC estimation error from [30], [34] with same current profile (o).

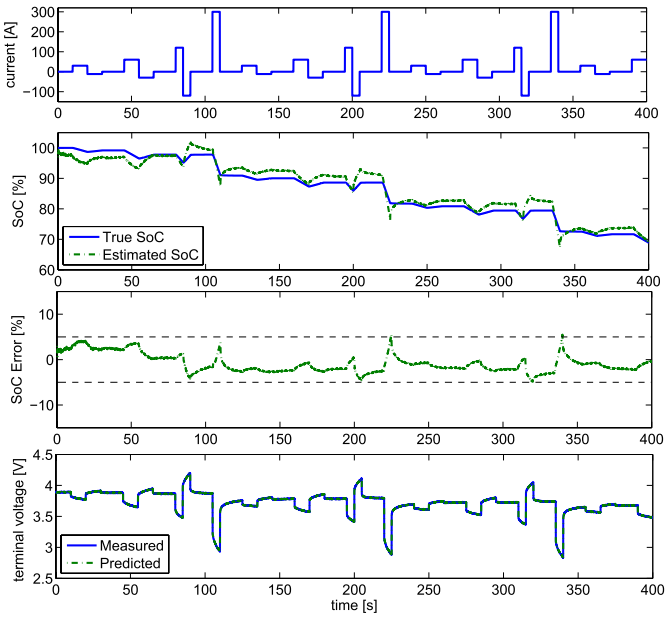

Fig. 13. SoC estimation results with a transient dis/charge current profile up to 50 C.

Electrochemical models are most beneficial at high current. The second excitation tests the observer for dis/charge current profile as high as 50 C. The results are shown in Fig. 13. The overall SoC RMS error is 2.3% and the maximum error 5.5%.

Having found satisfactory results, the time required per step by the proposed EKF algorithm is investigated. Fig. 14 shows the Kalman filter computation time as a function of the discretization along the x-axis. The linear complexity is experimentally confirmed. The advantages brought by the

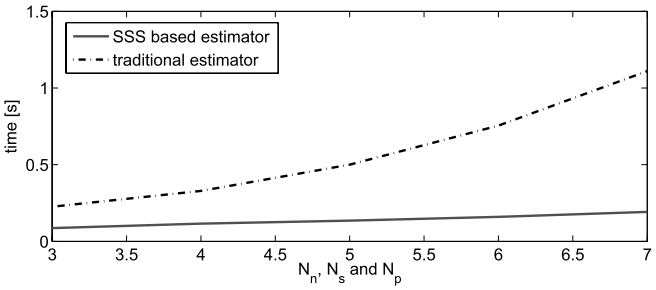

Fig. 14. Computational cost per step required by the efficient EKF algorithm for different discretization levels.

proposed computational schemes are evident with the possibility of reaching real-time estimation.

VI. Conclusion

The main contribution of this paper is the development of an efficient SoC estimation algorithm based on electrochemical equations for a Li-ion cell. Electrochemical models are known to be computationally prohibitive and thus their employment in BMS is difficult. In the present paper, a way of improving efficiency is presented.

The first part of this paper is devoted to showing how the fundamental electrochemical equations can be simulated in an efficient (i.e., $O(N)$), yet accurate way. Validation against a complete CFD model concludes that the model is sufficiently accurate. Besides being accurate and efficient, the control-oriented model has two other advantages. First, it is amenable to a state-space representation. The state-space representation can be easily exploited to design an SoC estimation algorithm. Second, the variables maintain their physical meaning. This potentially enables the estimation of several variables and not only SoC. Using these additional parameters, a more effective BMS can be built.

The second part of this paper presents the SoC estimation algorithm. A virtual-measurement-based method is presented to account for a local loss of observability. The virtual measures effectively incorporate heuristics in the algorithm. The algorithm is detailed and tested in two scenarios showing a maximum estimation error of 5%.

In this paper, Li-ion cells represent a real world, relevant application. However, the presented approach can be used for many other PDE systems or systems which are inherently spatially distributed in a string interconnected form. The gain in computational cost will be higher as the number of subsystems N grows, since traditional unstructured algorithms approach $O(N^3)$ computational complexity.

Appendix

In the linearization step, the system is first linearized and then lifted. Here it is shown that the lifting and linearization operations are indeed commutative. For brevity's sake consider a nonspatially strictly proper string interconnected system with two subsystems, described by (29). The linearization of the lifted system results in

$$A = \begin{bmatrix} \frac{\partial f_1}{\partial x_1} + \frac{\partial f_1}{\partial j_2}\frac{\partial j_2}{\partial x_1} & \frac{\partial f_1}{\partial j_2}\frac{\partial j_2}{\partial x_2} \\ \frac{\partial f_2}{\partial j_1}\frac{\partial j_1}{\partial x_1} & \frac{\partial f_2}{\partial x_2} + \frac{\partial f_2}{\partial j_1}\frac{\partial j_1}{\partial x_2} \end{bmatrix}$$

where

$$\frac{\partial j_2}{\partial x_1} = \left(\frac{Z_2^m}{1 - Z_1^p Z_2^m}\right)\frac{\partial g_{12}}{\partial x_1}, \quad \frac{\partial j_2}{\partial x_2} = \left(\frac{1}{1 - Z_1^p Z_2^m}\right)\frac{\partial g_{21}}{\partial x_2}$$
$$\frac{\partial j_1}{\partial x_1} = \left(\frac{1}{1 - Z_1^p Z_2^m}\right)\frac{\partial g_{12}}{\partial x_1}, \quad \frac{\partial j_1}{\partial x_2} = \left(\frac{Z_1^p}{1 - Z_1^p Z_2^m}\right)\frac{\partial g_{21}}{\partial x_2}. \tag{42}$$

On the other hand, the subsystem linearization will result into the following matrices:

$$A_1 = \frac{\partial f_1}{\partial x_1}, \quad B_1^p = \frac{\partial f_1}{\partial v_1^p} = \frac{\partial f_1}{\partial j_2} \quad \left(v_1^p = j_2(\cdot)\right), \quad C_1^m = \frac{\partial g_{12}}{\partial x_1}$$
$$A_2 = \frac{\partial f_2}{\partial x_2}, \quad B_2^m = \frac{\partial f_2}{\partial v_2^m} = \frac{\partial f_2}{\partial j_1} \quad \left(v_2^m = j_1(\cdot)\right), \quad C_2^p = \frac{\partial g_{21}}{\partial x_2}. \tag{43}$$

The system is not spatially strictly proper and thus cannot be lifted directly. It needs to be converted to a spatially strictly proper form using the technique shown in [25]. After this transformation and lifting, we obtain

$$A = \begin{bmatrix} A_1 + B_1^p\left(\frac{Z_2^m}{1-Z_1^p Z_2^m}\right)C_1^m & B_1^p\left(\frac{1}{1-Z_1^p Z_2^m}\right)C_2^p \\ B_2^m\left(\frac{1}{1-Z_1^p Z_2^m}\right)C_1^m & A_2 + B_2^m\left(\frac{Z_1^p}{1-Z_1^p Z_2^m}\right)C_2^p \end{bmatrix}. \tag{44}$$

Clearly (42) and (44) are equivalent.

References

[1] L. Lu, X. Han, J. Li, J. Hua, and M. Ouyang, "A review on the key issues for lithium-ion battery management in electric vehicles," *J. Power Sources*, vol. 226, pp. 272–288, Mar. 2013.

[2] B. Scrosati, J. Hassoun, and Y.-K. Sun, "Lithium-ion batteries. A look into the future," *Energy & Environ. Sci.*, vol. 4, no. 9, pp. 3287–3295, 2011.

[3] M. Armand and J.-M. Tarascon, "Building better batteries," *Nature*, vol. 451, no. 7179, pp. 652–657, 2008.

[4] A. Sciarretta, M. Back, and L. Guzzella, "Optimal control of parallel hybrid electric vehicles," *IEEE Trans. Control Syst. Technol.*, vol. 12, no. 3, pp. 352–363, May 2004.

[5] S. S. Codec and F. P. Spagnol, *Lithium-Ion Batteries for Electric Vehicles. Characterization, Modeling, State-of-Charge Estimation and Disequalization Phenomena*. Broderick, CA, USA: VDM Verlag, 2010.

[6] M. Charkhgard and M. Farrokhi, "State-of-charge estimation for lithium-ion batteries using neural networks and EKF," *IEEE Trans. Ind. Electron.*, vol. 57, no. 12, pp. 4178–4187, Dec. 2010.

[7] G. L. Plett, "Kalman-filter SoC estimation for LiPB HEV cells," in *Proc. CD-ROM Proc. 19th EVS*, Busan, Korea, Oct. 2002, pp. 1–12.

[8] T. F. Fuller, M. Doyle, and J. Newman, "Simulation and optimization of the dual lithium ion insertion cell," *J. Electrochem. Soc.*, vol. 141, no. 1, pp. 1–10, 1994.

[9] F. Fuller, M. Doyle, and J. Newman, "Simulation and optimization of the dual lithium ion insertion cell," *J. Electrochem. Soc.*, vol. 141, no. 1, pp. 1–10, 1994.

[10] G. L. Plett, "Extended Kalman filtering for battery management systems of LiPB-based HEV battery packs: Part 3. State and parameter estimation," *J. Power Sources*, vol. 134, no. 2, pp. 277–292, 2004.

[11] A. J. Salkind, C. Fennie, P. Singh, T. Atwater, and D. E. Reisner, "Determination of state-of-charge and state-of-health of batteries by fuzzy logic methodology," *J. Power Sources*, vol. 80, nos. 1–2, pp. 293–300, 1999.

[12] M. Verbrugge and P. Liu, "Electrochemical characterization of high-power lithium ion batteries using triangular voltage and current excitation sources," *J. Power Sources*, vol. 174, no. 1, pp. 2–8, 2007.

[13] M. Chen and G. Rincon-Mora, "Accurate electrical battery model capable of predicting runtime and iv performance," *IEEE Trans. Energy Convers.*, vol. 21, no. 2, pp. 504–511, Jun. 2006.

[14] N. Chaturvedi, R. Klein, J. Christensen, J. Ahmed, and A. Kojic, "Algorithms for advanced battery-management systems," *IEEE Control Syst., Mag.*, vol. 30, no. 3, pp. 49–68, Jun. 2010.

[15] P. Arora, M. Doyle, and R. White, "Mathematical modeling of the lithium deposition overcharge reaction in lithium-ion batteries using carbon-based negative electrodes," *J. Electrochem. Soc.*, vol. 146, no. 10, p. 3543, 1999.

[16] W. Gu and C. Wang, "Thermal and electrochemical coupled modeling of a lithium-ion cell, in lithium batteries," *J. Electrochem. Soc.*, vol. 147, no. 8, pp. 2910–2922, 2000.

[17] N. Chaturvedi, R. Klein, J. Christensen, J. Ahmed, and A. Kojic, "Algorithms for advanced battery-management systems," *IEEE Control Syst. Mag.*, vol. 30, no. 3, pp. 49–68, Jan. 2010.

[18] K. A. Smith, C. D. Rahn, and C.-Y. Wang, "Control oriented 1D electrochemical model of lithium ion battery," *Energy Convers. Manag.*, vol. 48, no. 9, pp. 2565–2578, 2007.

[19] L. Cai and R. White, "Reduction of model order based on proper orthogonal decomposition for lithium-ion battery simulations," *J. Electrochem. Soc.*, vol. 156, no. 3, p. A154, 2009.

[20] V. Subramanian, V. Boovaragavan, V. Ramadesigan, and M. Arabandi, "Mathematical model reformulation for lithium-ion battery simulations: Galvanostatic boundary conditions," *J. Electrochem. Soc.*, vol. 156, no. 4, p. A260, 2009.

[21] K. Smith, C. Rahn, and C. Wang, "Model order reduction of 1D diffusion systems via residue grouping," *J. Dyn. Syst., Meas., Control*, vol. 130, no. 1, p. 011012, 2008.

[22] O. Barbarisi, F. Vasca, and L. Glielmo, "State of charge Kalman filter estimator for automotive batteries," *Control Eng. Pract.*, vol. 14, no. 3, pp. 267–275, 2006.

[23] D. Di Domenico, G. Fiengo, and A. Stefanopoulou, "Lithium-ion battery state of charge estimation with a Kalman filter based on a electrochemical model," in *Proc. IEEE Int. CCA*, Sep. 2008, pp. 702–707.

[24] S. J. Moura, N. A. Chaturvedi, and M. Krstic., "Constraint management in li-ion batteries: A modified reference governor approach," in *Proc. ACC*, 2013, pp. 5352–5357.

[25] J. K. Rice and M. Verhaegen, "Distributed control: A sequentially semi-separable approach for spatially heterogeneous linear systems," *IEEE Trans. Autom. Control*, vol. 54, no. 6, pp. 1270–1283, Jun. 2009.

[26] S. Santhanagopalan and R. E. White, "Online estimation of the state of charge of a lithium ion cell," *J. Power Sources*, vol. 161, no. 2, pp. 1346–1355, 2006.

[27] S. Santhanagopalan and R. E. White, "State of charge estimation using an unscented filter for high power lithium ion cells," *Int. J. Energy Res.*, vol. 34, no. 2, pp. 152–163, 2010.

[28] S. Moura, N. Chaturvedi, and M. Krstic, "Adaptive PDE observer for battery soc/soh estimation via an electrochemical model," in *Proc. ASME Dyn. Syst. Control Conf.*, 2012, pp. 1–10.

[29] D. D. Domenico, G. Fiengo, and A. Stefanopoulou, "Lithium-ion battery state of charge estimation with a kalman filter based on a electrochemical model," in *Proc. IEEE Int. Conf. Control Appl.*, Sep. 2008, pp. 702–707.

[30] K. A. Smith, C. D. Rahn, and C.-Y. Wang, "Model-based electrochemical estimation of lithium-ion batteries," in *Proc. 17th IEEE Int. Conf. Control Appl.*, Sep. 2008, pp. 714–719.

[31] K. Smith and C.-Y. Wang, "Solid-state diffusion limitations on pulse operation of a lithium ion cell for hybrid electric vehicles," *J. Power Sources*, vol. 161, no. 1, pp. 628–639, 2006.

[32] J. C. Forman, S. Bashash, J. L. Stein, and H. K. Fathy, "Reduction of an electrochemistry-based li-ion battery model via quasi-linearization and padé approximation," *J. Electrochem. Soc.*, vol. 158, no. 2, pp. A93–A101, 2011.

[33] R. D'Andrea and G. E. Dullerud, "Distributed control design for spatially interconnected systems," *IEEE Trans. Autom. Control*, vol. 48, no. 9, pp. 1478–1495, Sep. 2003.

[34] K. Smith, C. Rahn, and C.-Y. Wang, "Model-based electrochemical estimation and constraint management for pulse operation of lithium ion batteries," *IEEE Trans. Control Syst. Technol.*, vol. 18, no. 3, pp. 654–663, May 2010.